

# Anisotropic Conductivity of Nodal Line Semimetal in Single-Component Molecular Conductor [Pd(dddt)<sub>2</sub>]

Yoshikazu Suzumura\*

*Department of Physics, Nagoya University, Chikusa-ku, Nagoya 464-8602, Japan*

Using a tight-binding model, we theoretically examine the anisotropic conductivity of the nodal line semimetal of a three-dimensional Dirac electron in a single-component molecular conductor [Pd(dddt)<sub>2</sub>], which consists of four molecules with HOMO and LUMO orbitals per unit cell. The conductivity shows an anisotropy given by  $\sigma_y > \sigma_x > \sigma_z$  in accordance with that of the velocity of the Dirac cone where  $z$  is the interlayer direction and  $y$  is the molecular stacking direction. With increasing pressure, the nodal line semimetal emerges, followed by a loop of the Dirac point where  $\sigma_x$  takes its maximum at a pressure. Such a pressure dependence is studied by calculating the density of states and chemical potential. The temperature dependence of anisotropic conductivity is examined at low temperatures to obtain a constant behavior, which is ascribed to the Dirac electron. The relevance of the present calculation to the experiment is discussed.

## 1. Introduction

Two-dimensional massless Dirac fermions are interesting topics as shown by the quantum Hall effect in graphene.<sup>1)</sup> Extensive studies on Dirac electrons have been explored in molecular conductors which are characteristic as the bulk system.<sup>2,3)</sup> In the organic conductor,  $\alpha$ -(BEDT-TTF)<sub>2</sub>I<sub>3</sub><sup>4)</sup> (BEDT-TTF=bis(ethylenedithio)tetrathiafulvalene), a two-dimensional Dirac electron with a tilted Dirac cone was found<sup>5)</sup> by noting the vanishing of the density of states at the Fermi surface.<sup>6)</sup> The Dirac point was calculated using the tight-binding model with the transfer energy estimated by the extended Hückel method,<sup>7)</sup> and the existence was verified by the electronic structure of first-principles calculation.<sup>8)</sup> Such a Dirac electron explains well the transport experiment under pressure.<sup>9,10)</sup>

A single-component molecular conductor [Pd(dddt)<sub>2</sub>] (dddt = 5,6-dihydro-1,4-dithiin-2,3-dithiolate) exhibits Dirac electrons owing to its almost constant resistivity at low temperatures and under pressure.<sup>11)</sup> The Dirac cone located between the conduction and valence bands was found by first-principles calculation<sup>12)</sup> and examined using a tight-binding model under pressure,<sup>3)</sup> which is described by an 8 x 8 matrix Hamiltonian with the energy band  $E_\gamma(\mathbf{k})$ , [ $\gamma=1$ (top), c, 8(bottom)]. The crystal consists of four molecules per unit cell with the HOMO and LUMO orbitals, which are symmetric and antisymmetric around the inversion center of the Pd atom, respectively. In contrast to the organic conductor, this material provides a line of the Dirac point in the three-dimensional momentum space  $\mathbf{k} = (k_x, k_y, k_z)$ , where there are transfer energies along the interlayer direction ( $k_z$ ) in addition to the intralayer plane of  $k_x$  and  $k_y$ . At ambient pressure, the insulating state is obtained since the chemical potential, owing to the half-filled band, is located in a gap between the LUMO and HOMO bands. Under high pressure, the Dirac point emerges between  $E_4(\mathbf{k})$  and

$E_5(\mathbf{k})$  when the HOMO band becomes larger than the LUMO band at  $\mathbf{k} = 0$ . The Dirac point gives a loop in the three-dimensional Brillouin zone.<sup>13)</sup> The Dirac electron in [Pd(dddt)<sub>2</sub>] is exotic since the Dirac point originates from the combined effect of the intralayer and interlayer transfer energies. The gap function of  $E_4(\mathbf{k}) - E_5(\mathbf{k})$ , where the zero gap gives a loop of the nodal line of the Dirac point, forms a contour with a cylindrical shape along the line suggesting a nodal line semimetal in three-dimensional momentum space.<sup>14,15)</sup> However, the property of such a semimetal is not yet clear owing to the complicated treatment of the chemical potential located on the loop, although isotropic property of such a system is partly known from the magnetic susceptibility.<sup>16)</sup> Thus, it is of interest to examine the anisotropic behavior of electric conductivity, which originates from the three-dimensional loop.

In this study, such a property of the Dirac electron is examined by calculating electric conductivity, which is useful for understanding the experiment on resistivity under pressures.<sup>11)</sup> In Sect. 2, the model and formulation are given. In Sect. 3, a loop of the Dirac point located between the conduction and valence bands is shown for typical pressures. Anisotropic conductivity for such a semimetal is examined by varying pressure. A maximum conductivity as a function of pressure is obtained and analyzed using the density of states. The effect of temperature is also calculated. Section 4 is devoted to the summary and discussion.

## 2. Model and Formulation

A single component molecular conductor [Pd(dddt)<sub>2</sub>] consists of four kinds of molecules (1, 2, 3, and 4) with HOMO and LUMO orbitals in the unit cell,<sup>3)</sup> and has a crystal structure with two kinds of layers where layer 1 includes molecules 1 and 3, and layer 2 includes molecules 2 and 4. Transfer energies, which are given by pairs between nearest-neighbor molecules, are as follows. The

\*E-mail: suzumura@s.phys.nagoya-u.ac.jp

interlayer energies in the  $x$ - $y$  plane are given by  $a$  (1 and 2 molecules, and 3 and 4 molecules) and  $c$  (1 and 4 molecules, and 2 and 3 molecules). The intralayer energies are given by  $p$  (1 and 3 molecules) and  $q$  (2 and 4 molecules) and  $b$  (perpendicular to the  $x$ - $z$  plane) being the largest one.

On the basis of the crystal structure,<sup>3)</sup> we examine a tight-binding model Hamiltonian given by

$$H = \sum_{i,j=1}^N \sum_{\alpha,\beta} t_{i,j;\alpha,\beta} |i, \alpha\rangle \langle j, \beta|, \quad (1)$$

where  $i$  and  $j$  are the sites of the unit cell with  $N$  being the total number of the square lattice, and  $\alpha$  and  $\beta$  denote the 8 molecular orbitals given by HOMO ( $H1, H2, H3, H4$ ) and LUMO ( $L1, L2, L3, L4$ ). The lattice constant is taken as unity. There are three kinds of transfer energies,  $t_{i,j;\alpha,\beta}$ , given by HOMO-HOMO (H), LUMO-LUMO (L), and HOMO-LUMO (HL).

The transfer energies  $t_{i,j;\alpha,\beta}(P)$  at a pressure  $P$  (GPa) are estimated using linear interpolation between two pressures of  $P = 8$  and  $0$  GPa, which are given by

$$t_{i,j;\alpha,\beta}(P) = r t_{i,j;\alpha,\beta}(0) + (1-r) t_{i,j;\alpha,\beta}(P_0), \quad (2)$$

with  $r = P/P_0$  and  $P_0 = 8$  GPa. The transfer energy in the unit of eV is given in Appendix. The pressure, where the behavior of the Dirac electron has been observed experimentally, corresponds to  $P=8$  GPa in the first-principles calculation.<sup>3)</sup>

Using the Fourier transform  $|\alpha(\mathbf{k})\rangle = \sum_j \exp[-i\mathbf{k}\mathbf{r}_j] |j, \alpha\rangle$  with a wave vector  $\mathbf{k} = (k_x, k_y, k_z)$ , Eq. (1) is rewritten as

$$H = \sum_{\mathbf{k}} |\Phi(\mathbf{k})\rangle \hat{H}(\mathbf{k}) \langle \Phi(\mathbf{k})|, \quad (3)$$

where the base is given by  $\langle \Phi(\mathbf{k})| = (\langle H1|, \langle H2|, \langle H3|, \langle H4|, \langle L1|, \langle L2|, \langle L3|, \langle L4|)$ , and  $\hat{H}(\mathbf{k})$  is the Hermite matrix Hamiltonian. The matrix element  $[\hat{H}(\mathbf{k})]_{\alpha,\beta}$  is given in Appendix.<sup>3,13)</sup> Since the symmetry of the HOMO (LUMO) is odd (even) with respect to the Pd atom, the matrix element of H-L (H-H and L-L) is the odd (even) function with respect to  $\mathbf{k}$ , i.e., an inversion symmetry at the time reversal invariant momentum. The energy band  $E_j(\mathbf{k})$  and the wave function  $\Psi_j(\mathbf{k})$ , ( $j = 1, 2, \dots, 8$ ) are calculated from

$$\hat{H}(\mathbf{k})\Psi_j(\mathbf{k}) = E_j(\mathbf{k})\Psi_j(\mathbf{k}), \quad (4)$$

where  $E_1 > E_2 > \dots > E_8$  and

$$\Psi_j(\mathbf{k}) = \sum_{\alpha} d_{j,\alpha}(\mathbf{k}) |\alpha\rangle, \quad (5)$$

with  $\alpha = H1, H2, H3, H4, L1, L2, L3$ , and  $L4$ . Noting that the band is half-filled owing to the HOMO and LUMO bands, we calculate a gap function defined by

$$E_g(\mathbf{k}) = \min[E_4(\mathbf{k}) - E_5(\mathbf{k})], \quad (6)$$

for all  $\mathbf{k}$  values in the Brillouin zone. The Dirac point  $\mathbf{k}_D$  is obtained from  $E_g(\mathbf{k}_D) = 0$ .

The electric conductivity is given as follows. Using the component of the wave function  $d_{\alpha\gamma}$  in Eq. (5), the re-

sponse function per spin is calculated as<sup>17)</sup>

$$\begin{aligned} \sigma^{\nu\nu'}(T) &= \frac{e^2}{\pi\hbar N} \sum_{\mathbf{k}} \sum_{\gamma,\gamma'} v_{\gamma\gamma'}^{\nu}(\mathbf{k})^* v_{\gamma\gamma'}^{\nu'}(\mathbf{k}) \int_{-\infty}^{\infty} d\epsilon \left( -\frac{\partial f(\epsilon)}{\partial \epsilon} \right) \\ &\times \frac{\Gamma}{(\epsilon - \xi_{\mathbf{k}\gamma'})^2 + \Gamma^2} \times \frac{\Gamma}{(\epsilon - \xi_{\mathbf{k}\gamma})^2 + \Gamma^2}, \end{aligned} \quad (7)$$

$$v_{\gamma\gamma'}^{\nu}(\mathbf{k}) = \sum_{\alpha\beta} d_{\alpha\gamma}(\mathbf{k})^* \frac{\partial \tilde{H}_{\alpha\beta}}{\partial k_{\nu}} d_{\beta\gamma'}(\mathbf{k}), \quad (8)$$

where  $\nu = x, y$ , and  $z$ .  $\hbar = 2\pi\hbar$  and  $e$  denote Planck's constant and the electric charge, respectively.  $\xi_{\mathbf{k}\gamma} = E_{\gamma}(\mathbf{k}) - \mu$  and  $\mu$  denotes the chemical potential obtained below.  $f(\epsilon) = 1/(\exp[\epsilon/T] + 1)$  with  $T$  being temperature in the unit of eV and  $k_B = 1$ . The damping constant  $\Gamma$  is introduced to obtain a finite conductivity where  $1/\Gamma$  corresponds to the lifetime by impurity scattering. The total number of lattice sites is given by  $N = N_x N_y N_z$ , and the lattice constant is taken as unity. At low temperatures, Eq. (7) is expanded as

$$\sigma^{\nu\nu'}(T) = \sigma^{\nu\nu'}(0) + C_{\nu\nu'}(T/\Gamma)^2 + \dots, \quad (9)$$

$$\begin{aligned} C_{\nu\nu'} &= \frac{e^2\pi}{12\hbar N} \sum_{\mathbf{k}} \sum_{\gamma,\gamma'} v_{\gamma\gamma'}^{\nu}(\mathbf{k})^* v_{\gamma\gamma'}^{\nu'}(\mathbf{k}) \Gamma^4 \\ &\left[ \frac{6\xi_{\mathbf{k}\gamma}^2 - 2\Gamma^2}{(\xi_{\mathbf{k}\gamma}^2 + \Gamma^2)^3(\xi_{\mathbf{k}\gamma'}^2 + \Gamma^2)} \right. \\ &+ \frac{4\xi_{\mathbf{k}\gamma}\xi_{\mathbf{k}\gamma'}}{(\xi_{\mathbf{k}\gamma}^2 + \Gamma^2)^2(\xi_{\mathbf{k}\gamma'}^2 + \Gamma^2)^2} \\ &\left. + \frac{6\xi_{\mathbf{k}\gamma'}^2 - 2\Gamma^2}{(\xi_{\mathbf{k}\gamma'}^2 + \Gamma^2)^3(\xi_{\mathbf{k}\gamma}^2 + \Gamma^2)} \right], \end{aligned} \quad (10)$$

where the first term of  $\sigma^{\nu\nu'}(T)$  is enough for  $T \ll \Gamma$ . The resistivity is given by  $1/\sigma^{\nu\nu'}$  since  $\sigma^{\nu\nu'}(T)$  for  $\nu \neq \nu'$  is much smaller than that for  $\nu = \nu'$  in the present numerical calculation. We mainly examine the electric conductivity at  $T=0$  with  $\nu = \nu'$ , ( $\nu = x, y, z$ ) while  $C_{\nu\nu} = C_{\nu}$  will be examined later to elucidate the  $T$  dependence. The first term of Eq. (9) is rewritten as

$$\sigma^{\nu\nu}(0) = \sigma_{3D}^{\nu} = \frac{1}{N_z} \sum_{k_z} \sigma_{2D}^{\nu}(k_z), \quad (11)$$

$$\begin{aligned} \sigma_{2D}^{\nu}(k_z) &= \frac{e^2}{\pi\hbar N_x N_y} \sum_{k_x k_y} \sum_{\gamma\gamma'} |v_{\gamma\gamma'}^{\nu}(\mathbf{k})|^2 \\ &\times \frac{\Gamma}{\xi_{\mathbf{k}\gamma'}^2 + \Gamma^2} \times \frac{\Gamma}{\xi_{\mathbf{k}\gamma}^2 + \Gamma^2}, \end{aligned} \quad (12)$$

where  $\sigma_{2D}^{\nu}(k_z)$  denotes the conductivity on the plane with a fixed  $k_z$ . A semimetal is obtained owing to the variation of the energy of the Dirac point  $\epsilon_D(k_z)$  with respect to  $k_z$ . Equation (12) gives two-dimensional conductivity, which reduces to a universal conductivity in the case of the isotropic Dirac cone with the chemical potential being equal to  $\epsilon_D(k_z)$ .<sup>17)</sup> The conductivity increases when the chemical potential moves away from  $\epsilon_D(k_z)$ .<sup>18)</sup>

The chemical potential  $\mu$  is determined self-consistently from the half-filled condition, which is given by

$$\frac{1}{N} \sum_{\mathbf{k}} \sum_{\gamma} f[E_{\gamma}(\mathbf{k})] = \int_{-\infty}^{\infty} d\omega D(\omega) f(\omega) = 4, \quad (13)$$

where

$$D(\omega) = \frac{1}{N} \sum_{\mathbf{k}} \sum_{\gamma} \delta[\omega - E_{\gamma}(\mathbf{k})]. \quad (14)$$

$D(\omega)$  denotes the density of states (DOS) per spin and per unit cell, which satisfies  $\int d\omega D(\omega) = 8$ . Note that Eq. (7) can be partly understood using DOS when  $\gamma = \gamma'$  and the  $\mathbf{k}$  dependence of  $v_{\gamma'\gamma}^{\nu}$  close to the Dirac point is small. The conductivity at  $T=0$  is analyzed using  $D(\omega)$ .

### 3. Conductivity of Dirac semimetal in [Pd(dddtt)<sub>2</sub>]

#### 3.1 Loop of Dirac point

The pressure dependence of the electronic states of [Pd(dddtt)<sub>2</sub>] is as follows. At ambient pressure, the insulating state is found where there exists a minimum gap at  $\mathbf{k} = (0, 0, 0)$ , and the LUMO bands ( $E_1, \dots, E_4$ ) are separated from the HOMO bands ( $E_5, \dots, E_8$ ). With increasing pressure ( $P$ ), the gap at  $\mathbf{k} = 0$  is reduced. When the minimum of the LUMO band becomes smaller than the maximum of the HOMO band, a Dirac point emerges between  $E_4(\mathbf{k})$  (conduction band) and  $E_5(\mathbf{k})$  (valence band) at around  $\mathbf{k} = 0$ . At the Dirac point given by  $E_4(\mathbf{k}) = E_5(\mathbf{k})$ , the H-L interaction (the coupling between HOMO and LUMO orbitals) vanishes owing to the orthogonality of the HOMO and LUMO wave functions.<sup>3)</sup> Thus, a loop of the Dirac point is obtained at the intersection of the plane of  $E_4(\mathbf{k}) = E_5(\mathbf{k})$  and that of the vanishing of the H-L interaction.<sup>13)</sup>

Figure 1(a) shows the Dirac point in the three-dimensional momentum space  $\mathbf{k} = (k_x, k_y, k_z)$  for  $P = 7.8$  and  $8.0$  GPa, which forms a loop in the region of almost the first Brillouin zone (inner loop) and that of the extended zone (outer loop), respectively. Since the critical pressure for the loop touching the boundary of the first Brillouin zone is given by  $P_c \simeq 7.79$ , the loop is already an extended one at the pressure of  $P = 8$  GPa where the behavior of the Dirac electron is found in the experiment on the resistivity.<sup>3)</sup> In Fig. 1(a), the Dirac point for the  $P = 8$  GPa is given by  $\mathbf{k}_D/\pi = (k_x/\pi, k_y/\pi, k_z/\pi) = (0, \pm 0.0875, 0)$  and  $(\pm 1.09, 0, \pm 1)$  on the plane of  $k_x$ - $k_y$  and  $k_z$ - $k_x$ , respectively. Note that the Dirac cone is anisotropic, e.g., the ratio of the velocity at  $P = 8$  GPa is estimated as  $v_x : v_y : v_z \simeq 1 : 5 : 0.2$ . The loop crosses both the plane of  $k_z = 0$  and  $k_y = 0$ . Figure 1(b) shows the Dirac point on the  $k_z$ - $k_x$  plane with some choices of pressure. The Dirac point shows  $k_x = 0$ , i.e., on the  $k_z$  axis for  $7.58 < P < 7.78$ , but deviates from  $k_x = 0$  for  $7.78 < P$  with a line,  $k_z/\pi - 1 \simeq -1.2k_x/\pi$ . The Dirac point also exists on the line of the  $k_x$  axis, which is a common feature of the loop. In the inset, the  $P$  dependence of the Dirac point  $\mathbf{k}_D = (0, k_y, 0)$  is shown where  $k_y \simeq 0.0182(P - 7.58)^{1/2}$ , suggesting the emergence of the Dirac point at  $P \simeq 7.58$  GPa.

#### 3.2 Conductivity

We take  $e = \hbar = 1$  in the following numerical calculation. The present system exhibits a nodal line semimetal owing to the variation of the energy in the Dirac point along the loop. Note that  $\epsilon_D$  depends slightly on  $k_z$  where  $\epsilon_D [= E_4(\mathbf{k}_D) = E_5(\mathbf{k}_D)]$ , and  $E_4(\mathbf{k}) > \epsilon_D(k_z) > E_5(\mathbf{k})$  for a fixed  $k_z$ . Such  $\epsilon_D$  of the Dirac point at  $P = 8$  GPa is shown in Fig. 1(c) corresponding to the nodal line of the outside loop of Fig. 1(a), where  $\delta E (= \epsilon_D - \mu)$ , and  $k_z$  is given as the function of  $k_x$  and  $k_y$ . For  $P = 8$  GPa, the energy  $\epsilon_D(k_z/\pi)$  as a function of  $k_z$  shows the relation  $\epsilon_D(0) < \mu < \epsilon_D(1.09)$ , where  $\epsilon_D(0) = 0.5540$ ,  $\epsilon_D(1.09) = 0.5570$ , and  $\mu = 0.5560 \simeq \epsilon_D(0.65)$ . The dispersion of  $\epsilon_D(k_z)$  with a width of  $\simeq 0.003$  suggests the electron and hole pockets along the line of the Dirac point, i.e., a semimetallic state. In this section, the property of such a Dirac electron is examined by calculating the electric conductivity mainly at  $T = 0$ .

In Fig. 2,  $\sigma_{\nu} (= \sigma_{3D}^{\nu})$  for  $P = 8$  GPa is shown as a function of  $\Gamma$ . The rapid increase in  $\sigma_{\nu}$  with decreasing  $\Gamma$  occurs as a competition between  $\Gamma$  and the deviation of  $\mu$  from  $\epsilon_D$ . In fact, the increase in  $\sigma_{\nu}$  occurs when  $|\mu - \epsilon_D|$  becomes larger than  $\Gamma$  for a single Dirac cone.<sup>18)</sup> In the case of Fig. 2, the increase is found for  $\Gamma$  being smaller than  $\langle |\delta\mu| \rangle_{av}$ , where  $\langle |\delta\mu| \rangle_{av}$  denotes the average of  $|\epsilon_D(k_z) - \mu|$  with respect to  $k_z$ . The characteristic of the Dirac electron where  $\sigma_{\nu}$  becomes constant is seen for a large  $\Gamma$ .<sup>18)</sup> Another aspect of the Dirac electron is seen from the component of  $\sigma_{\nu}$ , which consists of the interband contribution ( $\gamma \neq \gamma'$ ) and intraband contribution ( $\gamma = \gamma'$ ). Note that  $\gamma, \gamma' = 4$  and  $5$  is sufficient in the present calculation. When  $\langle |\delta\mu| \rangle_{av}$  is larger than  $\Gamma$ , the intraband contribution is dominant. When  $\langle |\delta\mu| \rangle_{av}$  is much smaller than  $\Gamma$ , the interband contribution becomes nearly equal to the intraband contribution. Such a crossover from small  $\Gamma$  to large  $\Gamma$  is shown for  $\sigma_x$ , where  $\sigma_{intra}$  is compared with  $\sigma_{inter}$ . Thus, in the present calculation of the conductivity, we take  $\Gamma = 0.002$ , which is a reasonable magnitude to find the Dirac behavior in the tight-binding model of [Pd(dddtt)<sub>2</sub>].

The conductivity of the nodal line semimetal is essentially determined by electrons close to the loop of the Dirac point. To comprehend the contribution of the respective location of the loop, we examine  $\sigma_{2D}^{\nu}(k_z)$  given by Eq. (12), which shows two-dimensional behavior associated with the Dirac cone on the plane of fixed  $k_z$ . Figure 3 shows  $\sigma_{\nu} = \sigma_{2D}^{\nu}(k_z)$  for  $P = 8$  GPa as a function of  $k_z$  in the reduced zone, i.e., the loop is folded at  $k_z = \pi$ . The constant behavior of  $\sigma_x$  for  $k_z/\pi < 0.5$  suggests that the Dirac cone is robust on the  $k_x$ - $k_y$  plane, and the increase in  $\sigma_x$  for  $0.6 < k_z/\pi < 1$  occurs owing to the rotation of the cone into the  $k_z$ - $k_x$  plane [outer loop shown by Fig. 1(a)], resulting in an increase in the density of the Dirac point per  $k_z$ . Note that the ratio of  $\sigma_{2D}^{\nu}(\pi)/\sigma_{2D}^{\nu}(0)$  for  $\nu = x$  is larger than that for  $\nu = y$ . From an effective model of the  $2 \times 2$  Hamiltonian of the Dirac cone with zero doping,<sup>18)</sup> the ratio of the conductivity is given by  $\sigma_x/\sigma_y \simeq (v_x/v_y)^2$ , where  $v_x$  and  $v_y$  are the velocities of the Dirac cone along  $k_x$  and  $k_y$  directions, respectively. The Dirac cone on the  $k_x$ - $k_y$  plane at  $k_z/\pi = 0$  shows

the velocity  $v_x \simeq 0.016$  eV and  $v_y \simeq 0.10$  eV, while the cone on the  $k_z$ - $k_x$  plane at  $k_y/\pi = 0$  shows  $v_x \simeq 0.019$  eV and  $v_z \simeq 0.0037$  eV. These velocities are estimated from the gap function of  $E_g(\mathbf{k})$  shown in Figs. 2(b) and 2(d) of Ref. 16. For  $k_z \simeq 0$ , the ratio  $\sigma_y/\sigma_x$  obtained from Fig. 3 (dotted and solid lines) is about half of that expected from the effective model. This difference may come from the fact that the chemical potential is located above  $\epsilon_D$ , i.e., corresponding to the apex of the cone. For  $k_z/\pi \simeq 0.91$  (i.e., 1.09 corresponding to the extended zone) the ratio of  $\sigma_x/\sigma_z$  obtained from Fig. 3 (solid and dashed lines) is nearly equal to that expected from the effective model of the Dirac cone on the  $k_z$ - $k_x$  plane. Thus, it turns out that  $\sigma_x$  exhibits a reasonable behavior of the nodal semimetal since  $\sigma_x$  comes from all the Dirac points on the loop. The inset denotes  $\sigma_x(k_z)$  for  $P = 7.6, 8.0$ , and  $8.2$ . The peak of  $\sigma_x$  for  $P=7.6$  is seen at  $k_z = 0$  since the corresponding loop is small and located at around  $\mathbf{k} = 0$ . For  $P=8$  and  $8.2$ , the peak is seen at  $k_z = \pi$  owing to the loop in the extended Brillouin zone. The fact that  $\sigma_x$  at  $P=8.2$  is smaller than that at  $P=8$  for an arbitrary  $k_z/\pi$  suggests a reduction in the density of states, as will be shown later.

In Fig. 4, the pressure dependence of  $\sigma_\nu (= \sigma_{3D}^\nu)$  ( $\nu = x, y$ , and  $z$ ) is shown with  $\Gamma = 0.002$ . The relation  $\sigma_y > \sigma_x > \sigma_z$  is the same as that in Fig. 3. At  $P=7.5$ ,  $\sigma_y$  and  $\sigma_z$  reduce sufficiently but a small  $\sigma_x$  remains where  $\Gamma$  is smaller than the insulating gap  $E_g \simeq 0.004$  for  $P = 7.5$ . With increasing  $P (> 7.58)$ ,  $\sigma_\nu$  increases owing to the increase of the loop. The increase of  $\sigma_y$  is much larger than those of  $\sigma_x$  and  $\sigma_z$ . A crossover from the insulating state to the semimetallic state is seen in  $\sigma_x$  for  $P \sim 7.6$ , while  $\sigma_y$  and  $\sigma_z$  show a monotonic increase. Note that  $\sigma_x$  takes a maximum at  $P \sim 8.1$ . The inset denotes the  $P$  dependences of  $\sigma_x$  for  $\Gamma = 0.0005$  and  $0.01$  and that of the chemical potential  $\mu$ . For a smaller  $\Gamma$ , the magnitude of the peak becomes larger, as is also seen from Fig. 2. Such characteristic pressure ( $\simeq 8.1$ ) for the peak is almost independent of  $\Gamma$ , and the peak moves to a cusp in the limit of small  $\Gamma$ . Since  $\langle |\delta\mu| \rangle_{av}$  is larger than  $\Gamma$ , such a peak is attributable to the intraband contribution suggesting a significant role of the nodal line semimetal. The chemical potential also shows a maximum at  $P \sim 7.8$  and decreases linearly with further increase in pressure, e.g.,  $\mu \simeq 0.5540$  at  $P = 8.5$ .

To examine the maximum  $\sigma_{3D}^x$ , we calculate the density of states  $D(\omega)$  given by Eq. (14). Figure 5 shows  $D(\omega)$  for the fixed  $P=7.8, 8.0$ , and  $8.2$ , where  $\omega = 0$  corresponds to the respective chemical potential. The minimum  $D(\omega)$  is located slightly above the chemical potential. At lower pressures, insulating behavior is obtained, e.g.,  $D(0) = 0$  for  $P < 7.58$  and a gap is given by  $E_g \simeq 0.004$  at  $P=7.5$ . At  $P = 7.6$ ,  $D(\omega)$  with  $\omega < 0$  is smaller than that with  $\omega > 0$ . Such a difference reduces with increasing pressure. At  $P = 8.2$ ,  $D(\omega)$  with  $\omega > 0$  decreases in addition to the decrease in  $D(0)$ , suggesting optimum electrons close to the chemical potential at around  $P = 8$ . In fact, the quantity given by  $\int D(\omega)d\omega$  in the interval range of  $-0.002 < \omega < 0.002$  is large for  $P=8.0$  compared with that for  $P=7.6$  and  $8.2$ . A quantity

that is estimated from Eqs. (11) and (12) without  $v_{\gamma\gamma'}(\mathbf{k})$  also shows a maximum at  $P \simeq 7.9$ . Thus, the pressure dependence of  $\sigma_{3D}^x$  is reasonably understood in terms of DOS except for the interband contribution. By noting a similar peak for the  $P$  dependences of  $D(0)$  and  $\mu$ , the peak of  $\sigma_{3D}^x$  at  $P \simeq 8.1$ , which is slightly larger than that of  $D(0)$  and  $\mu$ , may be a combined effect of  $v_{\gamma\gamma'}(\mathbf{k})$  and a factor given by  $(\xi_{\mathbf{k}\gamma'}^2 + \Gamma^2)^{-1}(\xi_{\mathbf{k}\gamma}^2 + \Gamma^2)^{-1}$  in Eq. (7) where the former increases slightly with increasing  $P$ .

Finally we examine the temperature ( $T$ ) dependence of  $\sigma_{3D}^\nu$ , which shows an increase proportional to  $T^2$ , as shown by Eq. (10). Figure 6 shows the pressure dependence of the coefficient  $C_\nu$  where the relation  $C_y > C_x > C_z$  is the same as that of  $\sigma_\nu$ . Similarly to  $\sigma_{3D}^x$ , there is a maximum  $C_x$  at  $P \simeq 8$ , and  $C_y$  shows a monotonical increase. Comparing Fig. 6 with Fig. 4, it is found that the first term of Eq. (9) becomes comparable to the second term of Eq. (9) for  $T \simeq \Gamma$ . Thus,  $\sigma_\nu \sim \text{const.}$  (i.e., independent of  $T$ ) is expected for  $T \ll \Gamma$ . In the inset,  $C_x$  corresponding to  $\Gamma = 0.001$  (solid line) and  $0.0005$  (dashed line) is shown for comparison. There is a similarity in the  $P$  dependence of  $C_x$  between these three  $\Gamma$ 's since the ratio of  $C_x$  at  $\Gamma = 0.002, 0.001$ , and  $0.0005$  is approximately given by 2:1:0.5. The second term of Eq. (9) becomes larger for a smaller  $\Gamma$ . This behavior, which is similar to the  $\Gamma$  dependence of  $\sigma_x$  in Fig. 2, can be understood qualitatively using the effective model of a  $2 \times 2$  Hamiltonian of the Dirac cone with the linear dispersion.<sup>18)</sup>

#### 4. Summary and Discussion

We examined electric conductivity for a nodal line semimetal in [Pdddt]<sub>2</sub> under pressure using a tight-binding model. The semimetal comes from the chemical potential located on the loop of the Dirac point between the conduction and valence bands [ $E_4(\mathbf{k})$  and  $E_5(\mathbf{k})$ ]. From the gap function  $E_g(\mathbf{k}) = E_4(\mathbf{k}) - E_5(\mathbf{k})$ , where the Dirac point is given by  $E_g(\mathbf{k}_D) = 0$ , the velocity of the Dirac cone is estimated to understand electric conductivity, which is determined by electrons near the loop. There is a large anisotropy of the conductivity given by  $\sigma_y > \sigma_x > \sigma_z$ , where  $y$  denotes the direction of the stacking of molecules and  $z$  is the interlayer direction. The contour of  $E_g(\mathbf{k})$  is an ellipse with anisotropic velocities of the Dirac cone, e.g.,  $v_x \simeq 0.016$  eV and  $v_y \simeq 0.10$  eV at  $k_z/\pi = 0$  ( $v_x \simeq 0.019$  eV and  $v_z \simeq 0.0037$  eV at  $k_y/\pi = 0$ ). The anisotropy of the conductivity comes from the anisotropy of the velocity, e.g.,  $\sigma_x/\sigma_y \sim v_x^2/v_y^2$ . The moderate magnitude of the damping constant  $\Gamma$  is taken to obtain a finite conductivity. The constant resistivity at low temperature ( $T$ ) is expected from the coefficient  $C_x$  [Eq. (10)] when  $T < \Gamma$ . The pressure ( $P$  GPa) dependence of conductivity was evaluated in the interval range of  $7.6 < P < 8.2$  to show a maximum at  $P \simeq 8.1$ . Such behavior of the conductivity was examined using the density of states around the chemical potential. The maximum, which is associated with a loop of the Dirac point, comes from the fact that the loop increases but the density of states decreases with increasing pressure.

Here, we note the energy dependence of the nodal line



located around the chemical potential, which is shown in Fig. 1(c). There is a noticeable difference in the energy dependence between  $\epsilon_D > \mu$  and  $\epsilon_D < \mu$ . This may be useful for further studies on the orbital magnetization in the present material, which is a possible topological (quasi) response inherent to a nodal line.<sup>19)</sup>

Finally, we comment on the experiment where the resistivity becomes independent of temperature under a given pressure. This behavior may be relevant to the Dirac electron since such a temperature independence of electric conductivity at low temperatures is also obtained theoretically for the nodal line semimetal of [Pd(dddtdt)<sub>2</sub>] as shown by Eq. (9) and in Fig. 6.

### Acknowledgements

The author thanks R. Kato for useful discussions, and M. Ogata for useful comments. This work was supported by JSPS KAKENHI Grant Number JP15H02108.

### Appendix: Matrix elements of Hamiltonian $\hat{H}(\mathbf{k})$

On the basis of  $\langle \Phi(\mathbf{k}) | = (\langle H1 |, \langle H2 |, \langle H3 |, \langle H4 |, \langle L1 |, \langle L2 |, \langle L3 |, \langle L4 |)$ , which is rewritten as  $(\langle 1 |, \langle 2 |, \langle 3 |, \langle 4 |, \langle 5 |, \langle 6 |, \langle 7 |, \langle 8 |)$ , the matrix elements  $[\hat{H}(\mathbf{k})]_{i,j} = h_{i,j}$  ( $i, j = 1, \dots, 8$ ) in Eq. (3) are obtained as<sup>3,13)</sup>

$$h_{1,1} = h_{3,3} = 2b_{1H} \cos k_y, \quad (\text{A.1})$$

$$h_{1,2} = a_H(1 + e^{-i(k_x + k_y + k_z)}), \quad (\text{A.2})$$

$$h_{1,3} = p_H(1 + e^{-ik_y} + e^{-ik_x} + e^{-i(k_x + k_y)}), \quad (\text{A.3})$$

$$h_{1,4} = c_H(1 + e^{ik_z}), \quad (\text{A.4})$$

$$h_{1,5} = b_{1HL}(e^{ik_y} - e^{-ik_y}), \quad (\text{A.5})$$

$$h_{1,7} = p_{1HL} + p_{2HLe}^{-ik_y} - p_{2HLe}^{-ik_x} - p_{1HLe}^{-i(k_x + k_y)}, \quad (\text{A.6})$$

$$h_{2,2} = h_{4,4} = 2b_{2H} \cos k_y, \quad (\text{A.7})$$

$$h_{2,3} = c_H(1 + e^{ik_z}), \quad (\text{A.8})$$

$$h_{2,4} = q_H(e^{i(k_x + k_z)} + e^{i(k_x + k_y + k_z)} + e^{ik_z} + e^{i(k_y + k_z)}), \quad (\text{A.9})$$

$$h_{2,5} = a_{HL}(1 - e^{i(k_x + k_y + k_z)}), \quad (\text{A.10})$$

$$h_{2,6} = b_{2HL}(e^{ik_y} - e^{-ik_y}), \quad (\text{A.11})$$

$$h_{2,7} = c_{HL}(e^{-ik_y} - e^{i(k_y + k_z)}), \quad (\text{A.12})$$

$$h_{2,8} = q_{1HLe}^{i(k_x + k_z)} + q_{2HLe}^{i(k_x + k_y + k_z)} - q_{2HLe}^{ik_z} - q_{1HLe}^{i(k_y + k_z)}, \quad (\text{A.13})$$

$$h_{3,4} = a_H(e^{ik_y} + e^{i(k_x + k_z)}), \quad (\text{A.14})$$

$$h_{3,5} = p_{2HL} + p_{1HLe}^{ik_y} - p_{1HLe}^{ik_x} - p_{2HLe}^{i(k_x + k_y)}, \quad (\text{A.15})$$

$$h_{3,7} = b_{1HL}(e^{ik_y} - e^{-ik_y}), \quad (\text{A.16})$$

$$h_{4,5} = c_{HL}(e^{-ik_y} - e^{i(k_y - k_z)}), \quad (\text{A.17})$$

$$h_{4,6} = q_{2HLe}^{-i(k_x + k_z)} + q_{1HLe}^{-i(k_x + k_y + k_z)}$$

$$-q_{1HLe}^{-ik_z} - q_{2HLe}^{-i(k_y + k_z)}, \quad (\text{A.18})$$

$$h_{4,7} = a_{HL}(e^{-ik_y} - e^{-i(k_x + k_z)}), \quad (\text{A.19})$$

$$h_{4,8} = b_{2HL}(e^{ik_y} - e^{-ik_y}), \quad (\text{A.20})$$

$$h_{5,5} = h_{7,7} = \Delta E + 2b_{1L} \cos k_y, \quad (\text{A.21})$$

$$h_{5,6} = a_L(1 + e^{-i(k_x + k_y + k_z)}), \quad (\text{A.22})$$

$$h_{5,7} = p_L(1 + e^{-ik_y} + e^{-ik_x} + e^{-i(k_x + k_y)}), \quad (\text{A.23})$$

$$h_{5,8} = c_L(e^{ik_y} + e^{i(-k_y + k_z)}), \quad (\text{A.24})$$

$$h_{6,6} = h_{8,8} = \Delta E + 2b_{2L} \cos k_y, \quad (\text{A.25})$$

$$h_{6,7} = c_L(e^{-ik_y} + e^{i(k_y + k_z)}), \quad (\text{A.26})$$

$$h_{6,8} = q_L(e^{i(k_x + k_z)} + e^{i(k_x + k_y + k_z)} + e^{ik_z} + e^{i(k_y + k_z)}), \quad (\text{A.27})$$

$$h_{7,8} = a_L(e^{ik_y} + e^{i(k_x + k_z)}), \quad (\text{A.28})$$

where  $h_{1,6} = h_{1,8} = h_{3,6} = h_{3,8} = 0$ , and  $h_{i,j} = h_{j,i}^*$ . We take eV as the unit of energy. The transfer energies  $t_{i,j;\alpha,\beta}$  in  $h_{i,j}$  are calculated from an interpolation formula, Eq. (2), where transfer energies at the following two pressures have been calculated using the extended Hückel method. At a pressure of  $P = 8$  GPa,<sup>3)</sup> ( $0$  GPa<sup>13)</sup>)  $t_{i,j;\alpha,\beta}$  is given by  $a_H = -0.0345(-0.0136)$ ,  $a_L = -0.0(-0.0049)$ ,  $a_{HL} = 0.0260(0.0104)$ ,  $b_{1H} = 0.2040(0.112)$ ,  $b_{1L} = 0.0648(0.0198)$ ,  $b_{1HL} = 0.0219(0.0214)$ ,  $b_{2H} = 0.0762(0.0647)$ ,  $b_{2L} = -0.0413(0.0)$ ,  $b_{2HL} = -0.0531(-0.0219)$ ,  $c_H = 0.0118(0.0)$ ,  $c_L = -0.0167(-0.0031)$ ,  $c_{HL} = 0.0218(0.0040)$ ,  $p_H = 0.0398(0.0102)$ ,  $p_L = 0.0205(0.0049)$ ,  $p_{1HL} = -0.0275(-0.0067)$ ,  $p_{2HL} = -0.0293(-0.0074)$ ,  $q_H = 0.0247(0.0067)$ ,  $q_L = 0.0148(0.0037)$ ,  $q_{1HL} = -0.0186(-0.0048)$ , and  $q_{2HL} = -0.0191(-0.0051)$ . The gap between the energy of HOMO and that of LUMO is taken as  $\Delta E = 0.696$  eV to reproduce the energy band by first-principles calculation.

- 1) K. S. Novoselov, A. K. Geim, S. V. Morozov, D. Jiang, M. I. Katsnelson, I. V. Grigorieva, S. V. Dubonos, and A. A. Firsov, *Nature* **438**, 197 (2005).
- 2) K. Kajita, Y. Nishio, N. Tajima, Y. Suzumura, and A. Kobayashi, *J. Phys. Soc. Jpn.* **83**, 072002 (2014).
- 3) R. Kato, H. B. Cui, T. Tsumuraya, T. Miyazaki, and Y. Suzumura, *J. Am. Chem. Soc.* **139**, 1770 (2017).
- 4) T. Mori, A. Kobayashi, Y. Sasaki, H. Kobayashi, G. Saito, and H. Inokuchi, *Chem. Lett.* **13**, 957 (1984).
- 5) S. Katayama, A. Kobayashi, and Y. Suzumura, *J. Phys. Soc. Jpn.* **75**, 054705 (2006).
- 6) A. Kobayashi, S. Katayama, K. Noguchi, and Y. Suzumura, *J. Phys. Soc. Jpn.* **73**, 3135 (2004).
- 7) R. Kondo, S. Kagoshima, and J. Harada, *Rev. Sci. Instrum.* **76**, 093902 (2005).
- 8) H. Kino and T. Miyazaki, *J. Phys. Soc. Jpn.* **75**, 034704 (2006).
- 9) K. Kajita, T. Ojio, H. Fujii, Y. Nishio, H. Kobayashi, A. Kobayashi, and R. Kato, *J. Phys. Soc. Jpn.* **61**, 23 (1992).
- 10) N. Tajima, M. Tamura, Y. Nishio, K. Kajita, and Y. Iye, *J. Phys. Soc. Jpn.* **69**, 543 (2000).
- 11) H. Cui, T. Tsumuraya, Y. Kawasaki, and R. Kato, presented at 17th Int. Conf. High Pressure in Semiconductor Physics (HPSP-17), 2016.

- |   |   |
|---|---|
| 12) T. Tsumuraya, H. Cui, T. Miyazaki, and R. Kato, presented at Meet. Physical Society Japan, 2014; T. Tsumuraya, H. Kino, R. Kato, and T. Miyazaki, in preparation for publication. | 17) S. Katayama, A. Kobayashi, and Y. Suzumura, J. Phys. Soc. Jpn. <b>75</b> , 023708 (2006). |
| 13) R. Kato and Y. Suzumura, J. Phys. Soc. Jpn. <b>86</b> , 064705 (2017).  | 18) Y. Suzumura, I. Igor, and M. Ogata J. Phys. Soc. Jpn. <b>83</b> , 023701 (2014).          |
| 14) S. Murakami, New J. Phys. <b>9</b> , 356 (2007).  | 19) S. T. Ramamurthy and T. L. Hughes, Phys. Rev. B <b>95</b> , 075138 (2017).                |
| 15) A.A. Burkov, M. D. Hook, and L. Balents, Phys. Rev. B <b>84</b> , 235126 (2011).  |   |
| 16) Y. Suzumura and R. Kato, Jpn. J. App. Phys. <b>56</b> , 05FB02 (2017).  |   |

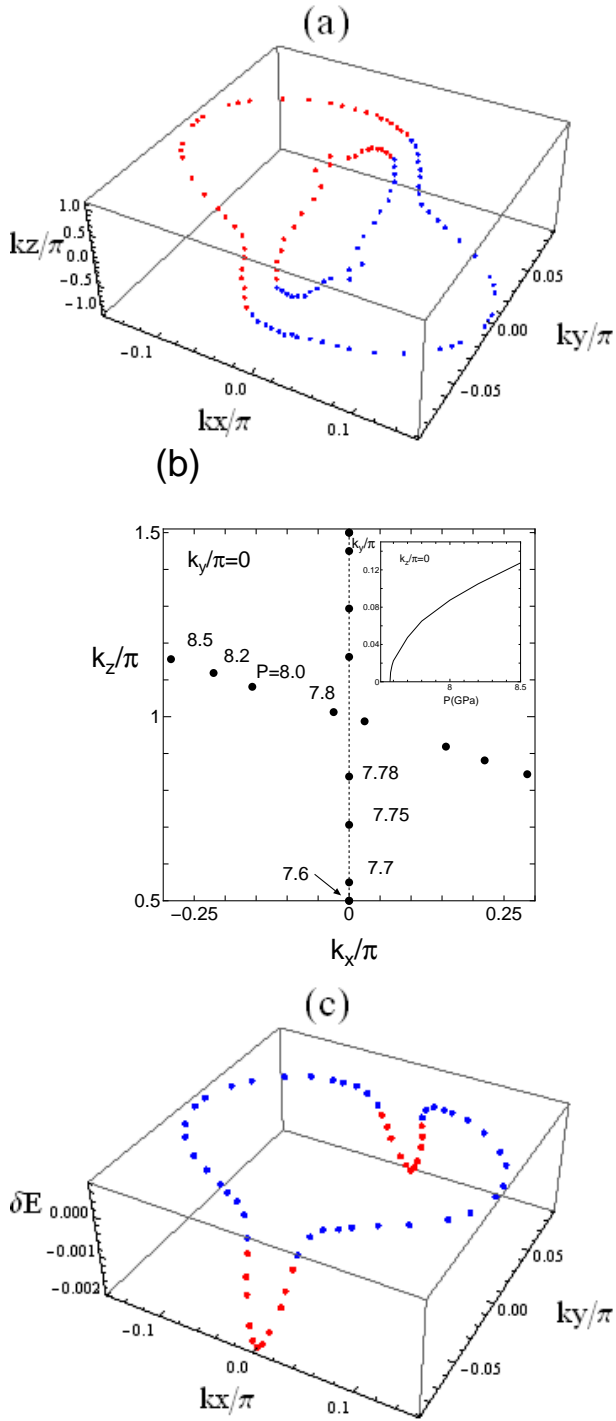


Fig. 1. (Color online) (a) 3D loop of Dirac point at  $P=7.8$  (inside) and 8 GPa (outside). The Dirac point is symmetric with respect to the origin  $(k_x, k_y, k_z) = (0, 0, 0)$ . (b) Dirac point on the plane of  $k_x$  and  $k_z$  where  $k_y = 0$  for  $7.58 < P < 7.79$  and  $|k_x| \neq 0$  for  $7.8 < P$ . The inset denotes the emergence of the Dirac point  $k_D$  as a function of  $P$  where  $k_x = k_z = 0$  and  $k_y \neq 0$  for  $P > 7.58$ . (c) Energy  $\epsilon_D$  of the Dirac point (at  $P=8$  GPa) on the plane of  $k_x$  and  $k_y$ , where  $\delta E = \epsilon_D - \mu$  and  $\mu \simeq 0.5560$ .

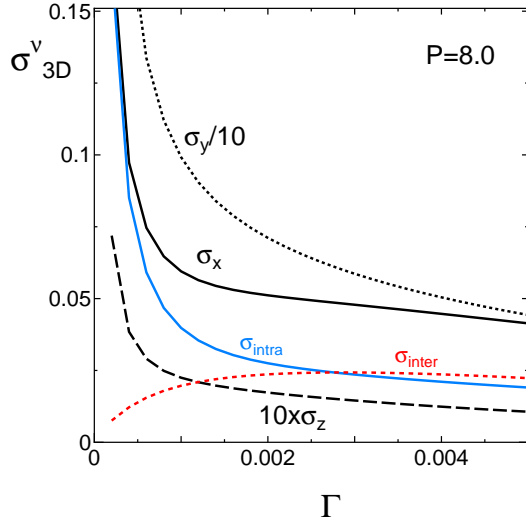


Fig. 2. (Color online)  $\Gamma$  dependence of conductivity  $\sigma_\nu = \sigma_{3D}^\nu$  ( $\nu = x, y$ , and  $z$ ) at  $P = 8$  GPa, where  $\sigma_y > \sigma_x > \sigma_z$ . The interband and intraband components are also shown for  $\sigma_x (= \sigma_{\text{intra}} + \sigma_{\text{inter}})$ .

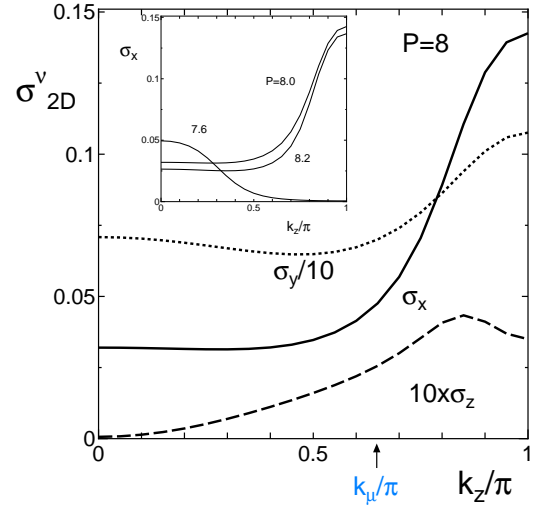


Fig. 3. (Color online)  $k_z$  dependence of conductivity  $\sigma_\nu = \sigma_{2D}^\nu$  ( $\nu = x, y$ , and  $z$ ) at  $P = 8$  GPa, where  $\sigma_y > \sigma_x > \sigma_z$ .  $\Gamma = 0.002$ .  $k_\mu$  denotes  $k_z$  corresponding to  $\epsilon_D(k_\mu) = \mu$ . The inset shows a comparison of  $\sigma_x(k_z)$  for  $P=8$  with those for  $P = 7.6$  and  $8.2$ , which correspond to the loop within the first Brillouin zone and extended Brillouin zone.



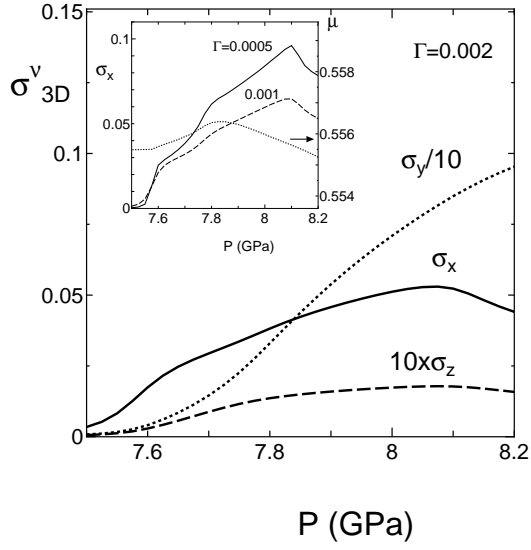


Fig. 4. Pressure dependences of  $\sigma_{3D}^\nu (= \sigma_\nu)$  for  $\sigma_x$ ,  $\sigma_y$  and  $\sigma_z$  for  $\Gamma = 0.002$ .  $\sigma_y > \sigma_x > \sigma_z$ . The inset shows the  $P$  dependences of  $\sigma_x$  for  $\Gamma = 0.0005$  (solid line) and  $0.001$  (dashed line), and that of the chemical potential  $\mu$  (dotted line).

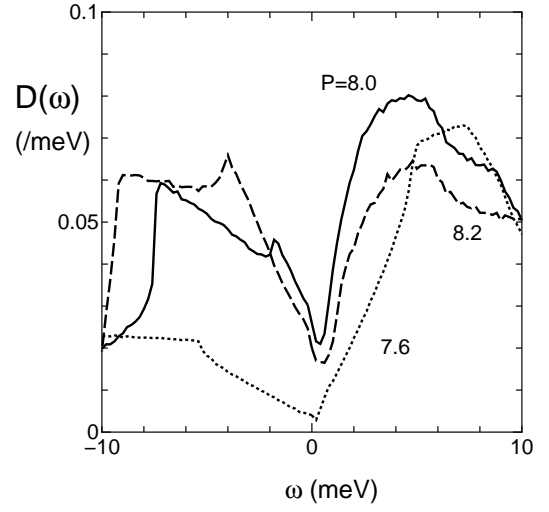


Fig. 5. Density of states  $D(\omega)$  for  $P = 7.6, 8, \text{ and } 8.2$  where the origin is taken as the respective chemical potential.

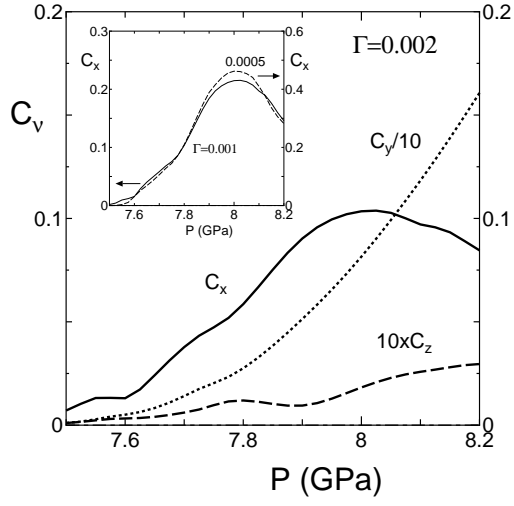


Fig. 6. Pressure dependence of coefficient of  $C_v$  for  $\Gamma = 0.002$  where  $\sigma_\nu(T) = \sigma_\nu(0) + C_\nu(T/\Gamma)^2$  and  $T$  denotes temperature in the unit of eV. The second term becomes comparable to the first term for  $T \simeq \Gamma$ . The inset denotes the corresponding  $C_x$  for  $\Gamma = 0.001$  (solid line) and  $0.0005$  (dashed line).